Design and Control of a Flying Manipulator with a Center of Gravity Adjusting Mechanism

WANG BO HANG*, AND WANG DAO BO*

* College of Automation Engineering Nanjing University of Aeronautics & Astronautics, Nanjing, China.
Authors E-mail:(bhwang@nuaa.cn, dbwangpe@nuaa.edu.cn)

ABSTRACT

In order to solve the problem of COG (Center of Gravity) shift caused by grasping, handling and other tasks of operational flying robot, this research proposes a working flying robot with COG adjustment mechanism. This article also offers a COG adjustment control strategy. Through the kinematics derivation of the manipulator in the operating device, the strategy dynamically calculates the change of the COG position of the compound system during the motion of the manipulator. The paper calculates the rotation angle of the adjusting mechanism by using the torque balance equation, which helps adjust the COG of the composite system. In order to verify the effectiveness of the proposed control strategy, this paper studies the influence of manipulator motion on the COG trajectory and fixed-point hovering position of the composite system with or without COG adjustment control. Outdoor physical experiments are carried out to test the flying robot carrying load. This study also analyzes the stability effect of the adjusting mechanism in the fixed-point hovering operation. The experimental results show that under the control strategy, the COG adjusting mechanism can adjust the offset of the COG of the compound system in real time during the operation of the flying robot, which verifies the effectiveness of the control strategy.

Key Words: Flying Manipulator, Gravity Center Adjusting Control, Rotor-Flying Manipulator, Flying Manipulation, Quadrotor.

1. INTRODUCTION

In recent years, UAVs (Unmanned Aerial Vehicle) have been the focus of research in the military and commercial fields due to their stable structure, flexible maneuverability, and autonomous flight. They are widely used in aerial surveys, pesticide spraying, plant protection, and target tracking [1-3]. Compared with the mobile operation of ground mobile robots, UAVs equipped with operating devices have expanded the operating space to 3D (Three-Dimensional), broadening the application fields of UAVs, handling dangerous goods in complex environments, placing and recycling survey equipment, and aerial target grabbing and other aspects have broad application prospects. This kind of composite system is called an operational flying robot [4].

In early research, researchers installed simple robotic grippers on the bottom of the aircraft to grip and carry objects. This kind of operating device has a simple structure and is easy to control [5-7]. One review paper has exhaustively discussed the many types of single and multi-UAV grippers [8]. In one study, the researcher used passive mechanical compliance and adaptive under-actuation in a gripper to allow for large positional displacements between the aircraft and target object [9]. However, these studies lack a sophisticated robotic arm system. Therefore, their operational flexibility is limited, which is not conducive to the completion of more complex tasks. In order to meet the operational requirements of different tasks, researchers installed special designed robotic arms to complete tasks such as grasping and handling, placing pipes, rotating valves, and opening doors and drawers. In contact with the environment, the flying robot is affected by the environment and the operated object, which shifts the COG of the composite system, causing the flying robot to be unstable and even crash [10]. One research analyzed the relationship between the stability of the aircraft and the distance from the centroid of the system's COG and proved that the larger the mass of the carried object, the smaller the distance allowed by the carried object to deviate from the centroid of the flying platform [11].

In view of the shift of the COG, one researcher proposed a flying robot that collects plant tree crowns. The flying robot had controllers, batteries, and other components at the rear of the rotorcraft. The front end of the fuselage extends two rod-mounted mechanical arms. Through reasonable assembly of the components, the COG of the aircraft is controlled near the geometric center of the aircraft. The method is only applicable to the case where the operating device is relatively small compared to the aircraft and the grasped object is relatively small relative to the overall mass of the system. Another study used the battery as a component to adjust the COG, and a simple mechanism was installed in the middle of the fuselage of the flying robot to enable the battery to move back and forth parallel to the forward direction of the aircraft, thereby adjusting the position of the COG in that direction. This method adds a counterweight that can be moved horizontally, but requires a large space under the fuselage, and has a limited moving distance, slow movement, and untimely adjustment. One study proposed a full-state LQR (Linear Quadratic Regulator) control strategy. The results show that the LQR controller has a good stabilization effect when the system is in equilibrium and the manipulator moves in a small range, but the controller cannot stabilize the system when the swing

amplitude of the manipulator is large [12-13]. In another research, by establishing the kinematics and dynamics model of the system, the COG coordinate position is dynamically calculated. Aiming at the COG compensation term, a dynamic COG compensation control method based on inversion method is proposed, which improves the performance of position and attitude tracking of flying robot. One study considered the motion of the robotic arm as a disturbance, and proposed a gain-adjustable PID (Proportional Integral Derivative) control. The results show that the method has a good stabilization effect on the motion of the robotic arm, but does not analyze the effect under different load conditions. Another study treats the operating device as a part of the aircraft for overall dynamics modeling, and proposes an enhanced adaptive controller that uses an online parameter estimation algorithm to enable the flying robot to complete autonomous handling of unknown loads.

Considering the aircraft and the operating device as a whole, the design of the nonlinear control strategy based on the dynamic model has significant impact, but the modeling is difficult and the control is complicated. In order to simplify modeling and control, this paper proposes a flying robot with a COG adjustment mechanism and its control strategy. Based on the kinematics and dynamics modeling of the flying robot, the relationship between the change of the COG of the composite system and the movement of the manipulator is analyzed, and the position of the COG of the composite system and the angle of rotation of the COG adjustment mechanism are dynamically calculated. Physical experiments verify the effectiveness of the COG control strategy.

The rest of the study is as follows: Section 2 presents the mechanism design and various parameters of the composite system. While, section 3 offers the kinematic modeling, kinetic modeling, and the COG control strategy. Whereas, section 4 deals with the testing platform, COG estimation, and the physical experiment. Section 5 concludes the whole study. In the end, section 6 presents the future work.

2. MECHANISMS DESIGN

The structure of the operational flying robot system with gravity center adjustment mechanism proposed in this paper is shown in Fig. 1. The total mass of the flying robot is 2.5 kg. Table 1 shows the parameters of each part of the composite system.

FIG. 1. SYSTEM STRUCTURE OF THE FLYING MANIPULATOR

TABLE 1. PARAMETERS OF THE COMBINED SYSTEM

Name	I_{xy} (kg.mm^2)	I_{xz} (kg.mm^2)	I_{yz} (kg.mm^2)
Upper segment of manipulator	0.045	0.069	-0.003
Lower segment of manipulator	0.000	5.525	0.000
Mechanical claw	0.002	-0.003	0.001
Center of gravity adjustment mechanism	0.000	0.000	0.000

The composite system is divided into two subsystems, namely the quadrotor on the upper part and the operating device on the lower part. The four-rotor aircraft has a wheelbase of 550 mm and a rated take-off mass of 3.2 kg. Two KV700 brushless motors are selected, and two pairs of 12-inch forward and reverse propellers are used to provide power. The flight controller uses 32-bit open source flight control hardware Pixhawk based on ARM chip. The flight control device has a built-in 3-axis accelerometer, gyroscope, magnetometer, and barometer sensor, and an external GPS (Global Positioning System) module is used to obtain aircraft position information, and communicate with the ground station through a 433 MHz wireless digital transmission device.

The operating device consists of a robotic arm, a COG adjustment mechanism, and a mechanical claw, and wirelessly communicates with the ground station through a ZigBee module. The CC2530 chip on the module is used as the processor of the COG adjustment controller, and the servo is controlled by the serial port to RS485 bus module.

Compared with the parallel structure robot arm, the series structure robot arm has a simpler structure, a larger working space, mature modeling and control methods. Therefore, the operating device in this paper uses a three DOF (Degree of Freedom) series robot arm. The robot arm has a mass of 215 g and a fully straightened length of 280 mm. It is responsible for tasks such as grasping and handling. A single DOF gravity center adjustment mechanism is designed to adjust the COG shift generated by the composite system during the operation of the robot arm in real time without hindering the work of the robot arm. The COG adjustment mechanism uses the battery as a counterweight, and adjusts the position COG of the composite system based on the position movement calculated by the COG adjustment controller. Considering the quality of the steering gear, output torque, and control accuracy, the joints of the operating device use RobotisDynamixel's RX-28 steering gear. The maximum output torque of the steering gear is 2.8 Nm. The body and each part of the bracket are processed by carbon fiber board and nylon according to different strength requirements.

This paper designs a claw-shaped end effector, and uses 2 miniature DC motors to drive the mechanical claws for expansion and contraction. The mechanical claw has a reverse self-locking function. After completing the task of grasping objects, there is no need to provide additional driving force to

maintain the gripping state. When the robot claw is fully opened, the distance is 75 mm. When it is closed, the distance from the wrist joint to the center of the claw is 55 mm.

3 MODELING AND CONTROL

3.1 Kinematic Modeling

Assuming that the body is a rigid body, the base system $\{O_i\}$ fixed on the ground is the inertial system, and $\{O_b\}$ is the body coordinate system. The origin of the body coordinate system $\{O_b\}$ is fixed at the centroid of the quadrotor. The positive direction of the x_b axis is the forward direction of the quadrotor. The z_b axis is perpendicular to the plane of the quadrotor.

Let $\mathbf{P} = [x, y, z]^T$ denote the position vector of the origin of the coordinate system $\{O_b\}$ in the coordinate system $\{O_i\}$, and $\mathbf{\Phi} = [\phi, \theta, \psi]^T$ denote the attitude vector of the coordinate system $\{O_b\}$ in the coordinate system $\{O_i\}$, where ϕ, θ, ψ denote the roll angle, pitch angle and yaw angle respectively. Let $\mathbf{V} = [u, v, w]^T$ is the linear velocity of coordinate system $\{O_b\}$ relative to coordinate system $\{O_i\}$ in coordinate system $\{O_i\}$, $\mathbf{\Omega} = [p, q, r]^T$ is the angular velocity of coordinate system $\{O_b\}$ relative to coordinate system $\{O_i\}$. $\mathbf{r}_G = [x_G, y_G, z_G]^T$ is the offset vector of the center of gravity of the composite system in coordinate system $\{O_b\}$. The rotation matrix from the body coordinate system to the inertial coordinate system is:

$$R = \begin{bmatrix} c\psi\psi c - s\varphi\varphi s\psi s & -c\varphi\varphi s & c\psi\psi s + c\theta\theta s\varphi s \\ c\theta\theta s + c\psi\psi s\varphi s & c\varphi\varphi c & s\psi\psi s - c\psi\psi c\theta s \\ -c\varphi\varphi s & s\varphi & c\varphi\varphi c \end{bmatrix} \quad (1)$$

Among them, c and s respectively represent cos and sin functions.

The D-H (Denavit-Hartenberg) method is used to model the operating system. $\{O_c\}$ and $\{O_j\}$ (j = 1,2,3) represent the joint coordinate system of the COG adjustment mechanism and each joint coordinate system of the robot arm, and $\{O_4\}$ is the coordinate system of the end effector, and its origin is fixed at the machine center position when the claw is closed. Table 2 shows the D-H parameters of the operating system (θ_j, d_j, α_{j-1}, a_{j-1}). $\{O_0\}$ and $\{O_{0'}\}$ represent the mounting coordinate systems of the robot arm and the COG adjustment mechanism, respectively. θ_j (j = 1,2,3) represents the rotation angle of each joint of the robotic arm, and θ_c represents the rotation angle of the joint of the gravity center adjustment mechanism. The rotation matrices of the mounting coordinate system of the robot arm and the center of gravity adjustment mechanism to the body coordinate system are:

$$A_0 = \begin{bmatrix} 0.707 & 0.707 & 0 & x_0 \\ 0 & 0 & -1 & y_0 \\ 0.707 & 0.707 & 0 & z_0 \\ 0 & 0 & 0 & 1 \end{bmatrix} A_{0'} = \begin{bmatrix} 0.707 & 0.707 & 0 & x_0 \\ 0 & 0 & -1 & y_0 \\ 0.707 & 0.707 & 0 & z_0 \\ 0 & 0 & 0 & 1 \end{bmatrix}$$

TABLE 2. D-H PARAMETERS OF THE MANIPULATION SYSTEM

Number	θ_j (o)	α_{j-1} (o)	α_{j-1} (mm)	d_j (mm)
0-1	θ_1	0	0	0
1-2	θ_2-90	0	ι_1	0
2-3	θ_3	90	0	ι_2
3-4	0	0	0	ι_3

Among them, $x_0 = 76.5$ mm, $y_0 = 0$, $z_0 = -74.5$ mm, $x_{0'} = -76.5$ mm, $y_{0'} = 0$, $z_{0'} = -74.5$ mm. Obtain the transformation matrix of each sub-coordinate system to the body coordinate system using:

$$^bT_j = A_0 A_1 ... A_j \quad (2)$$

Among them, the transformation matrix A_{j+1} from the coordinate system $\{O_{j+1}\}$ to $\{O_j\}$ is as follows

$$A_{j+1} = \begin{bmatrix} c\theta_{j+1} & -s\theta_{j+1} & 0 & a_j \\ s\theta_{j+1}c\alpha_j & c\theta_{j+1}c\alpha_j & -s\alpha_j & -d_{j+1}s\alpha_j \\ s\theta_{j+1}s\alpha_j & c\theta_{j+1}s\alpha_j & c\alpha_j & -d_{j+1}c\alpha_j \\ 0 & 0 & 0 & 1 \end{bmatrix} \quad (3)$$

A point p on the robotic arm is expressed as $\mathbf{P}^i_p$ in the sub-coordinate system $\{O_j\}$ of each part of the robotic arm, then p can be expressed as the body coordinate system $\{O_b\}$ as:

$$P_p^b = {}^bT_j P_p^j \quad (4)$$

Can be expressed in the inertial coordinate system $\{O_i\}$ as:

$$P_p^i = P + RP_p^b \quad (5)$$

3.2 Kinetic Modeling

Considering that the operating device remains static in the non-working stage, it moves only when working on the object, and the rotation speed of the joint is slow and adjustable, so the influence of the operating device on the power system is ignored and the system is regarded as a changing static state. In summary, the dynamics of the composite system is modeled under the static state, and its dynamic equation can be derived from the Newton-Euler method.

$$m\left[\ddot{P} + \dot{\Omega} \times r_G + \Omega \times (\Omega \times r_G)\right] = G + RF_p + RF_e \quad (6)$$

$$I_m \dot{\Omega} + \Omega \times I_m \Omega = M_P r_G \times F_P + M_e \quad (7)$$

Where m is the mass of the composite system and I_m is the inertia tensor. A four-rotor aircraft generates lift by rotating the

rotor. The lift and torque are related to the speed of rotation of the rotor, which is modeled as:

$$F_i = c_T \omega_i^2 \tag{8}$$

$$M_i = c_Q \omega_i^2 \tag{9}$$

Among them, c_T and c_Q are lift coefficient and torque coefficient, respectively, which are related to air density, propeller area and propeller diameter, and can be obtained through static thrust test. $\mathbf{F}_e$ and $\mathbf{M}_e$ are the forces and moments acting on the composite system from the external environment, $\mathbf{G} = [0,0,-mg]^T$ and $\mathbf{F}_p = [0,0,f_p]^T$ are the gravity and lift acting on the composite system, respectively. f_p= F1+F2+F3+F4 is the resultant force generated by the 4 propeller in the z direction. $\mathbf{M}_p = [\tau_x,\tau_y,\tau_z]^T$ is the torque acting on the composite system, and l is the length of the force arm. From this, the power distribution matrix of the composite system can be obtained:

$$\begin{bmatrix} f_p \\ \tau_x \\ \tau_y \\ \tau_x \end{bmatrix} = \begin{bmatrix} c_T & c_T & c_T & c_T \\ -c_T l & c_T l & c_T l & -c_T l \\ -c_T l & -c_T l & c_T l & c_T l \\ c_Q & -c_Q & c_Q & -c_Q \end{bmatrix} \begin{bmatrix} \omega_1^2 \\ \omega_2^2 \\ \omega_3^2 \\ \omega_4^2 \end{bmatrix} \tag{10}$$

In order to simplify the analysis, this paper focuses on the control of the shift of the COG when the manipulator carries a load, so that $\mathbf{F}_e$=0, $\mathbf{M}_e$=0. The system dynamics equations can be obtained from Equations (1,6-9).

$$\begin{cases} \dot{u} = \dfrac{f_p}{m}\left(\sin\theta\cos\psi + \cos\theta\sin\phi\sin\psi\right) + a_1 \\ \dot{v} = \dfrac{f_p}{m}\left(\sin\theta\sin\psi + \cos\theta\sin\phi\sin\psi\right) + a_2 \\ \dot{w} = \dfrac{f_p}{m}\cos\theta\cos\phi - g + a_3 \end{cases} \tag{11}$$

$$\begin{cases} a_1 = \left(q^2 + r^2\right)x_G + \left(r^2 + pq\right)y_G - z_G\left(\dot{q} + pr\right) \\ a_2 = \left(r^2 + pq\right)x_G + \left(p^2 + r^2\right)y_G + z_G\left(\dot{p} + qr\right) \\ a_1 = \left(\dot{q} - pr\right)x_G - \left(\dot{p} + qr\right)y_G + z_G\left(p^2 + q^2\right) \end{cases} \tag{12}$$

$$\begin{cases} \dot{p} = \dfrac{I_{yy} - I_{xx}}{I_{xx}}qr + \dfrac{\tau_x - y_G f_p}{I_{xx}} \\ \dot{q} = \dfrac{I_{zz} - I_{xx}}{I_{yy}}pr + \dfrac{\tau_y - x_G f_p}{I_{yy}} \\ \dot{r} = \dfrac{I_{yy} - I_{xx}}{I_{zz}}pq + \dfrac{\tau_z}{I_{zz}} \end{cases} \tag{13}$$

3.3 Center of Gravity Control Strategy

The purpose of gravity center adjustment control is to control the COG of the system near the z_b axis of the body coordinate system. In the composite system, the four-rotor aircraft is symmetrical, and the operating device is installed symmetrically about the $y_b o_b z_b$ plane and adjusted to the initial equilibrium state. Therefore, the COG of the composite system is shifted only when the robotic arm moves. In this case, the COG adjustment controller obtains the required rotation angle of the COG adjustment mechanism by calculating the change in the position of the COG of each part when the robot arm moves.

Fig. 2 is a flowchart of the data processing of the gravity center adjustment controller. The data processing mainly includes the following three steps:

Step-1 Initialization: The parameters mainly include the initial state, the angle of the joint of the robotic arm, the adjusting mechanism at the time of reset, the position of the COG of each part of the robotic arm in the respective sub-coordinate system, and the transformation matrix of each sub-coordinate system to the body coordinate system.

Step-2 Compare: The main purpose is to judge whether to process the sent data. If the target angle of the movement and the current angle are smaller than a set value, i.e. when the movement of the robot arm changes little, the system will default the adjustment mechanism to perform no operation.

Step-3: Calculate. Obtain the transformation matrix from the current sub-coordinate system to the previous sub-coordinate system. Calculate the position of the COG of each part in the body coordinate system {Ob} from Equations (2-5). Use the balance Equation (14) to derive the expression (15) of the controller of the adjustment mechanism, and calculate the target position of the movement of the adjustment mechanism of the COG. This information is updated each time the robot arm moves, and at the same time, the new position information is also fed back to the controller by the servo.

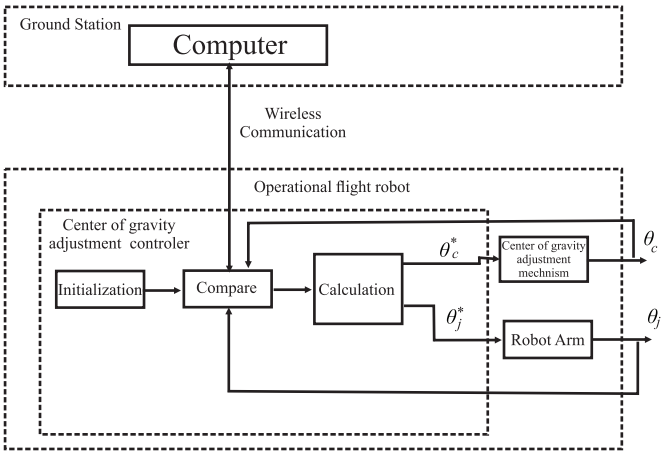

FIG. 2. FLOW CHART OF THE GRAVITY CENTER CONTROL

$$m_c x_c + m_g x_g + \sum_{j=1}^{3} m_j x_j = 0 \tag{14}$$

$$\theta_c = \frac{180}{\pi}\left(\frac{\pi}{4} + \arcsin\frac{m_g x_g + \sum_{j=1}^{3} m_j x_j}{a}\right) \tag{15}$$

Among them, m_j represents the weight of each part of the robot arm, and m_c and m_g represent the mass of the COG adjustment mechanism and the grasped object, respectively. x_j, x_c, and x_g represent the positions of the COG of each part on the x_b axis in the body coordinate system, $x_j = e_1\left({}^{b}T_j x_{jg}\right), x_g = e_1\left({}^{b}T_4 x_{gg}\right)$ and $e_1 = [1,0,0,0]$, x_{jg} is the x coordinate of the COG of the j^{th} part of the robot arm in the coordinate system $\{O_j\}$, x_{gg} is the x coordinate of the grabbing object in the coordinate system $\{O_4\}$, a, b are constants, It is related to the coordinates of the COG and mass of the adjustment mechanism in $\{O_c\}$. In this design, a = 56970 and b = 0.725. When $m_g = 0$, the joint angle of the COG adjustment mechanism can be obtained without load.

4. TESTS AND EXPERIMENTS

4.1 Testing Platform

Fig. 3 shows the structure of a testing system for a working flying robot. The trajectory generator and position controller generate the target position of the body ξ^* and attitude Φ^* and the target joint angle θ_j^* of the robot arm movement as system inputs. $\omega_1, \omega_2, \omega_3$, and ω_4 are the rotation speeds of the four brushless motors respectively. The attitude controller uses PID control to adjust the attitude of the robot. Equation (10) generates the lift force F_p and torque M_p that act on the composite system. The operating device controller controls the manipulator and the COG adjustment mechanism by formula (15).

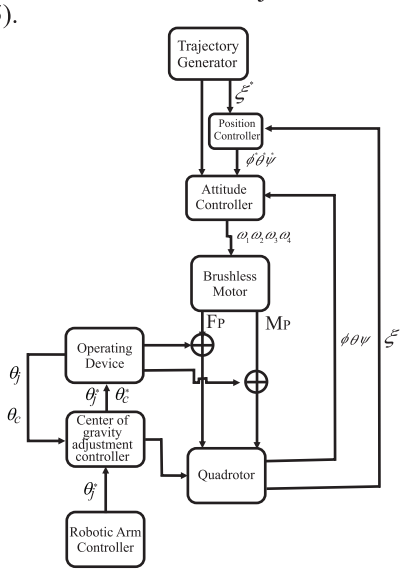

FIG. 3. STRUCTURE OF THE TESTING SYSTEM

The overall maneuverability of the operational flying robot system is tested. In the initial state of the robot, the joint angle of the robot arm $\theta_1 = -80^\circ, \theta_2 = 125^\circ, \theta_3 = 0^\circ$, and the joint angle of the adjustment mechanism $\theta_c = 57^\circ$. In the three experiments, the testing system made the flying robot take off in 2s, and the roll, pitch, and yaw signals were input in 3 experiments within 0-16 s. Experiments show that the PID controller can stably track the desired attitude and altitude in the absence of operation.

4.2 Center of Gravity Estimation

In the air operation system, m_i represents the mass of each part of the manipulator, m_0 represents the mass of the body, m_c represents the mass of the COG adjusting mechanism, and m_g represents the mass of the grasped object. As described in Section 3, the joint coordinate system of the manipulator and the joint coordinate system of the COG adjusting mechanism are represented by $\{O_j\}$ and $\{O_c\}$ respectively. The position of the COG of each part in the body coordinate system $\{O_b\}$ and the inertial coordinate system $\{O_i\}$ can be calculated by Equations (4-5). The COG of the composite system can be obtained from the centroid solution theory of multi-body mechanics.

$$T_G + \frac{m_c p_c + m_g p_g + \sum_{j=1}^{3} m_i p_i}{m_c + m_g + \sum_{i=0}^{3} m_i} \tag{16}$$

In the experiment, the joints of the manipulator are made to move according to the formula (17) given in Equation (17):

$$\begin{cases} \theta_1 = t - 90 \\ \theta_2 = 90 - t, 0 \le t \le 180 \\ \theta_3 = t, -90 \end{cases} \tag{17}$$

First, we test the composite system when the COG is adjusted. When the manipulator moves, the COG adjustment mechanism makes corresponding movements according to the angle calculated by the center adjustment controller, and controls the COG to change near the z_b axis of the body coordinate system. The maximum deviation distance is 0.1062 mm, the minimum deviation distance is 0.1036 mm, and the change range is 0.0026 mm. Then, we test the composite system without COG adjustment control. At this time, the manipulator moves and the COG adjustment mechanism maintains the initial stationary state. In this state, the COG of the composite system changes significantly. The maximum deviation distance from the z_b axis is 20.4535 mm, the minimum deviation distance is 13.8334 mm, and the variation range is 34.2896 mm. Comparing the two results, it can be seen that the COG adjustment mechanism can better control the COG shift of the composite system.

4.3 Physical Experiment

Conduct outdoor physical experiments to test the actual impact of the flight robot manipulator on the composite system. In the experiment, the attitude information and altitude information of the flying robot are fed back to the ground station in real time through the wireless data transmission device, and the flight controller records the flight data. Using a 2 cm diameter and 100 g tube as a load, the swing arm experiment was performed during aerial work. Fig. 4 is a

comparison diagram of fixed-point hovering swing arm with and without COG adjustment control under load. The robotic joint steering gear moves from $\theta_1 = -80^\circ, \theta_2 = 125^\circ, \theta_3 = 0$ to $\theta_1 = \theta_2 = \theta_3 = 0$, and then moves to $\theta_1 = 25^\circ$ at a speed of 40 r / min.,$\theta_2 = \theta_3 = 0$. In Fig. 4(a1-6), the time interval is 0.8 s and the flying robot is hovering near the starting point of the swing arm motion. Fig. 4(b1-6) show that when the time interval is 0.7 s and the flying robot uses only flight control for adjustment, the flying robot drifts with the movement of the manipulator and it is difficult to stabilize in the original position.

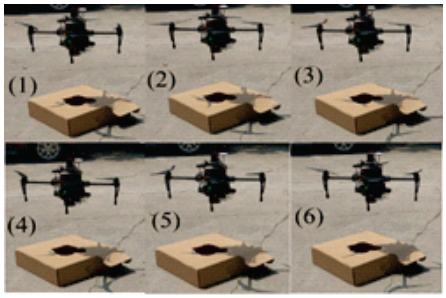

(a) CENTER OF GRAVITY ADJUSTMENT CONTROL

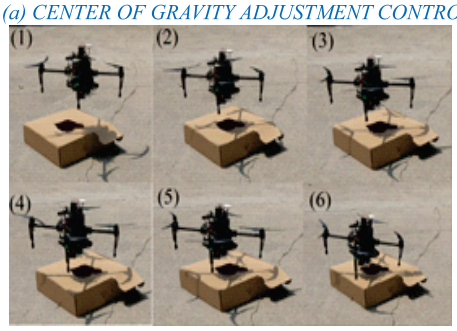

(b) NO CENTER OF GRAVITY ADJUSTMENT CONTROL

FIG. 4. HOVERING COMPARISON WITH OR WITHOUT THE GRAVITY CENTER ADJUSTING CONTROL

5. CONCLUSION

This paper designed a kind of operational flying robot with COG adjusting mechanism and established its kinematics and dynamics model. Based on the COG adjustment mechanism, this study proposed a COG adjustment control method. Through the analysis of the motion of the manipulator, the change of the COG position of the composite system was dynamically calculated, and the rotation angle needed to control the COG adjustment mechanism was obtained. The effectiveness of the design was verified by comparing the influence of the manipulator motion on the trajectory of the compound COG and the fixed-point hovering position with or without COG adjustment control. Outdoor experiments were carried out. It was preliminarily verified that the COG adjusting mechanism can better maintain the stability of the composite system during operation. Compared with the existing control methods and adjusting mechanisms, the modeling and control of the mechanism with COG adjustment was simple and feasible, the response was fast, and the manipulator had a large operable load.

6. FUTURE WORK

In the future, the platform control will be further optimized from the flight control algorithm, airborne cameras will be installed and visual servo systems will be introduced to realize the automatic grasping of the target object by the operating device.

AKNOWLEDGEMENT

The authors would like to express their immense gratitude to the faculty of the College of Automation Engineering Nanjing University of Aeronautics & Astronautics, Nanjing, China, for their huge support and help throughout this research. The authors would also like to offer their thanks to the anonymous referees for their valued comments and helpful suggestions for the improvement of this study.

REFERENCES

[1] Mukherjee, A., Misra, S., and Raghuwanshi, N.S., "A Survey of Unmanned Aerial Sensing Solutions in Precision Agriculture", Journal of Network and Computer Applications, pp. 102461, 2019.

[2] Jan, W., Augugliaro, F., Cadalbert, A., D'Andrea, R., Gramazio, F., and Kohler, M., "Aerial Robotic Construction Towards a New Field of Architectural Research", International Journal of Architectural Computing, Volume 10, No. 3, pp. 439-459, 2012.

[3] James, K.R., Stol, K.A., and Xu, W., "Aerial Manipulator Interactions with Trees for Canopy Sampling", IEEE/ASME Transactions on Mechatronics, Volume 23, No. 4, pp. 1740-1749, 2018.

[4] Petrescu, R.V.V., "Medical Service of Robots", Journal of Mechatronics and Robotics, Volume 3, pp. 60-81, 2019.

[5] Nie, J., Xiangyu, C., and Wang, Z.L., "Electrically Responsive Materials and Devices Directly Driven by the High Voltage of Triboelectric Nanogenerators", Advanced Functional Materials, Volume 29, No. 41, pp. 1806351, 2019.

[6] Shao, J.-Y., Cui, B.-B., Tang, J.-H., and Zhong, Y.-W., "Resistive Memory Switching of Transition-Metal Complexes Controlled by Ligand Design", Coordination Chemistry Reviews, Volume 393, pp. 21-36, 2019.

[7] Fan, M., Lifang, Z., Zhao, H., and Zhang, K.,"An Overview of Quadrotor UAV-Based Early Warning System of Landslide Hazards", 7th International Conference on Sustainable Energy and Environment Engineering, Atlantis Press, 2019.

[8] Abdullah, M., Tarek, T., Zweiri, Y., and Gan, D., "A Survey of Single and Multi-UAV Aerial Manipulation", Unmanned Systems, Volume 8, No. 2, pp. 119-147, 2020.

[9] Paul, P.E., and Dollar, A.M., "Aerial Grasping from a Helicopter UAV Platform", Experimental Robotics, pp. 269-283, Springer, Berlin, Heidelberg, 2014.

[10] Calderón, A.A., Chen, Y., Yang, X., Chang, L., Nguyen, X.-T., Singer, E.K., and Pérez-Arancibia, N.O., "Control of Flying Robotic Insects: A Perspective and Unifying Approach", arXiv Preprint arXiv:1910.11911, 2019.

[11] Spurný, V., Báča, T., Saska, M., Pěnička, R., Krajník, T., Thomas, J., Thakur, D., Loianno, G., and Kumar, V., "Cooperative Autonomous Search, Grasping, and Delivering in a Treasure Hunt Scenario by a Team of Unmanned Aerial Vehicles", Journal of Field Robotics, Volume 36, No. 1, pp. 125-148, 2019.

[12] Sun, N.,, Wu, Y., Chen, H., and Fang, Y., "Antiswing Cargo Transportation of Underactuated Tower Crane Systems by a Nonlinear Controller Embedded with an Integral Term", IEEE Transactions on Automation Science and Engineering, Volume 16, No. 3, pp. 1387-1398, 2019.

[13] Nekoo, S.R., "Digital Implementation of a Continuous-Time Nonlinear Optimal Controller: An Experimental Study with Real-Time Computations", International Society of Automation Transactions, 2020.